

Measuring extended red sensitivity in a $1.7\mu\text{m}$ -cutoff HgCdTe detector array

Ryan C. Terrien^{a,b,c}, Andrew J. Monson^{b,c}, Suvrath Mahadevan^{b,c}, Chad Bender^{b,c}, Samuel P. Halverson^{b,c}, and Larry Ramsey^{b,c}

^aNational Institute of Standards and Technology, 325 Broadway, Boulder, CO 80305, USA

^bThe Pennsylvania State University, 525 Davey Lab, University Park, PA 16802, USA

^cCenter for Exoplanets & Habitable Worlds, The Pennsylvania State University, University Park, PA 16802, USA

ABSTRACT

Infrared detectors with cutoff wavelengths of $\sim 1.7\mu\text{m}$ have much lower sensitivity to thermal background contamination than those with longer cutoff wavelengths. This low sensitivity offers the attractive possibility of reducing the need for fully cryogenic systems for YJH-band work, offering the potential for “warm-pupil” instrumentation that nonetheless reduces detected thermal background to the level of dark current. However, residual sensitivity beyond the cutoff wavelength is not well characterized, and may preclude the implementation of such warm-pupil instruments. We describe an experiment to evaluate the long-wavelength sensitivity tail of a $1.7\mu\text{m}$ -cutoff HAWAII-2RG array using a thermal blocking filter. Our results suggest the possibility of measurable red sensitivity beyond $\sim 2\mu\text{m}$. Ongoing improvements will confirm and refine this measurement. The thermal blocking filter offers the prospect of warm-pupil NIR instrument operation, which is particularly valuable for cost-effective and efficient testing systems: it has facilitated NIR detector characterization and will enable crucial laboratory tests of laser frequency comb calibration systems and other NIR calibration sources.

Keywords: near-infrared, detectors, thermal background

1. INTRODUCTION

Large format, low-noise, high quantum efficiency (QE) HgCdTe near-infrared (NIR) detector arrays¹ have already had a large impact on many areas of astronomy, and their implementation is increasingly widespread. This is partially due to the versatility of $\text{Hg}_{1-x}\text{Cd}_x\text{Te}$: the bandgap is tunable from $\sim 0 - 1.5\text{ eV}$ (cutoff wavelengths from $0.8 - 30\mu\text{m}$) by changing the relative proportion of Cd and Hg, while a consistent lattice size facilitates the growth of high-quality crystals.²

Thermal background radiation presents a significant challenge for the development and use of any NIR instrument. The thermal background itself, or noise on this signal, can easily drown out the signals of interest if not mitigated properly. With HgCdTe, careful selection of cutoff wavelength enables high sensitivity for in-band radiation and rejects out-of-band thermal background. For instruments that target the *H*-band and redder, in-band thermal background can be significant at room temperature, so they typically must be cryogenically cooled to suppress this background.

For very short-wave NIR work (*J*-band or bluer, $\lambda < 1.3\mu\text{m}$) an alternative is possible: the combination of a short detector cutoff ($\sim 1.7\mu\text{m}$) and a thermal blocking filter can enable sensitivity out to $\sim 1.3\mu\text{m}$ while suppressing thermal noise at redder wavelengths. Due to the steep rise of the thermal spectrum at longer

Further author information: (Send correspondence to R.C.T.)

R.C.T.: E-mail: ryan.terrien@nist.gov

Certain commercial equipment, instruments, or materials are identified in this paper in order to specify the experimental procedure adequately. Such identification is not intended to imply recommendation or endorsement by the National Institute of Standards and Technology, nor is it intended to imply that the materials or equipment identified are necessarily the best available for the purpose.

wavelengths, such a “warm pupil” system requires a thorough evaluation of the detector and filter efficiencies; any red leaks can easily dominate the detected signal. We describe here ongoing experiments aimed at quantifying the sensitivity tail of a 1.7 μm -cutoff Hawaii-2 RG (H2RG) using a high-quality thermal blocking interference filter.

1.1 The Urbach Tail

The energy limits of the valence and conduction bands in HgCdTe are not perfectly sharp: a tail of energy levels extends into the bandgap, resulting in absorption and detection of photons with energies lower than the band gap energy. These extra energy levels are known to result from disorder in the HgCdTe crystal.³ The corresponding absorption coefficient (α) obeys the empirical “Urbach” rule set forth in Ref. 4, and is typically parametrized as:

$$\alpha(E) = \alpha_0 e^{(E-E_0)/w}, \quad (1)$$

where α_0 is the absorption coefficient at the bandgap energy E_0 (taken here to be 500 cm^{-1} , the half peak value for a photosensitive layer approximately $10 \mu\text{m}$ thick), and w is a characteristic energy that represents the steepness of the Urbach tail. This absorption has been explored extensively in material studies of HgCdTe, and has been found to vary among individual crystals, and to have both composition and temperature dependence.^{2,3,5-7}

Although the nature of near-bandgap absorption in HgCdTe has been extensively studied, the properties and practical consequences of the Urbach tail for modern HgCdTe detector arrays are not well-understood. Most implementations are cooled to suppress the thermal background sufficiently that the details of the near-bandgap sensitivity are unimportant. However, the steepness of the Urbach tail has implications for the feasibility of a warm-pupil NIR system as described above: a longer tail places increasingly strong requirements on a thermal blocking optic. We describe here the design and initial results of an experiment to measure the properties of the Urbach tail in a 1.7 μm -cutoff H2RG detector array.

2. EXPERIMENTAL SETUP

The experiment is centered on an engineering-grade 1.7 μm cutoff Teledyne HgCdTe detector array.¹ This detector is installed in a GL Scientific (GLS) test cryostat. Through a custom thermal blocking interference filter (cold), the detector views a variable temperature blackbody source. We describe the components in detail below.

3. THE H2RG DETECTOR

The H2RG detector is controlled via a SIDECAR ASIC⁸ and the Teledyne-provided control software. For the tests discussed here, the reverse bias was approximately 250 mV.* The detector was operated with normal clocking, in unbuffered mode. We read out full frame reads using 32 output channels in both up-the-ramp and Fowler sample configurations.

For the purposes of this work, the quantum efficiency (QE) of the H2RG in the near-bandgap region is taken to be

$$QE(E) = 1 - e^{-\alpha(E)t}, \quad (2)$$

where t is the thickness of the photosensitive layer (assumed to be approximately $10 \mu\text{m}$). This assumes a quantum yield (number of conduction electrons created per photoelectric event) of unity, and that all such electrons are detected (see e.g., Ref 9).

For photons with $0.8 \leq \lambda \leq 1.7 \mu\text{m}$, the QE is a linear interpolation of measured values from the Teledyne test report for this detector. Example QE curves are shown in Figure 1.

*Bias settings: $V_{\text{reset}} = 0.3 \text{ V}$, $D_{\text{sub}} = 0.55 \text{ V}$, $V_{\text{biasgate}} = 1.9 \text{ V}$, $V_{\text{refmain}} = 1.7 \text{ V}$

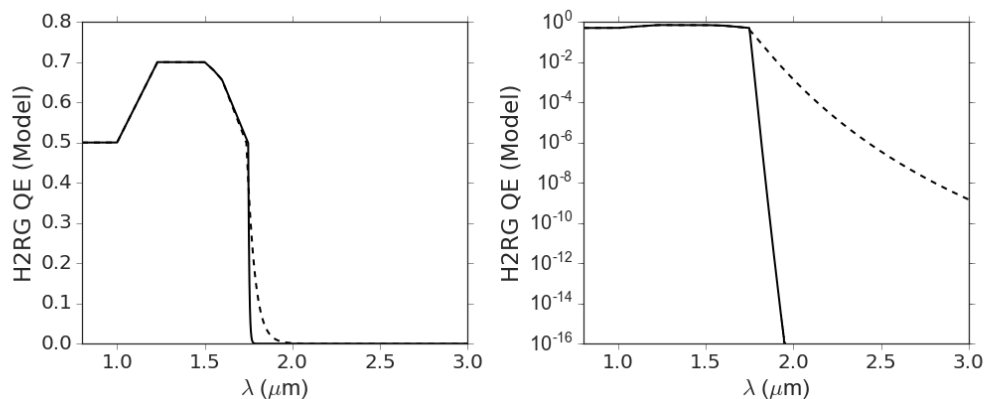


Figure 1. Example QE curves for the H2RG in linear (left) and logarithmic (right) space. Two extreme examples of Urbach tail parameters are shown.

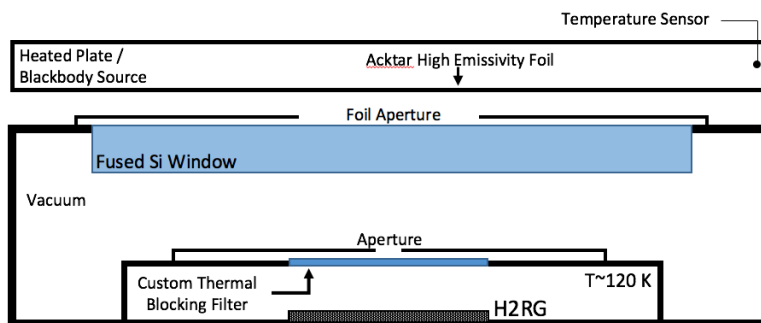


Figure 2. A schematic of the current H2RG test system. The detector is mounted inside the cooled “inner sanctum” of the GLS cryostat. The thermal blocking filter is potted into the inner sanctum lid, and a variable aperture is mounted immediately above this filter. The outer shell of the cryostat has a fused silica window, and above this is another thin variable aperture. Finally, the variable temperature heated lid is mounted on the top, and is covered with an Acktar black sheet to provide a blackbody emission spectrum.

3.1 The GLS Test Cryostat

The GLS cryostat itself is of a similar design to those used by Teledyne for detector testing. It is cubic, with about 30 cm to a side. Within the vacuum shell is a radiation shield, and within that is an actively-controlled so-called “inner sanctum.” The detector is mounted within the inner sanctum, near a SIDECAR ASIC,⁸ and both are connected to the cold finger of a Stirling cryocooler. The cryocooler maintains the cold finger at ~ 68 K, and the FPA and ASIC are actively controlled via resistive heaters and a Lakeshore temperature monitoring system. During operation, the FPA, ASIC, and inner sanctum are maintained at 120 K.

Outside the window of the GLS system, separated by a one-inch thick syrofoam thermal buffer, is a variable temperature plate, with a thermistor attached. The temperature of this plate can be varied from approximately -170 to 100 °C, using a reservoir of liquid nitrogen or a heater. Attached to the plate, visible to the H2RG, is a sheet of Acktar high-emissivity foil, which ensures a blackbody-like thermal spectrum while minimizing scattered light from this surface.

The detector views the blackbody surface through two variable apertures: one is mounted on the inner sanctum, a few mm above the thermal blocking filter, and one is mounted ~ 1 mm above the outer cryostat window.

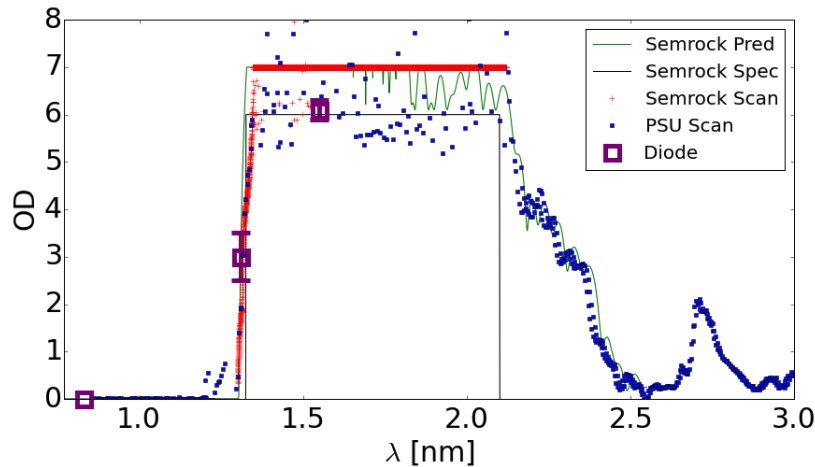


Figure 3. The transmission characteristics of the custom Semrock thermal blocking filter. The spec values are shown, along with predicted and measured performance provided by Semrock (as discussed in the text). The filter blocks strongly from 1.3 – 2.1 μm and maintains good transmission from 0.8-1.2 μm . All data shown are for normal incidence.

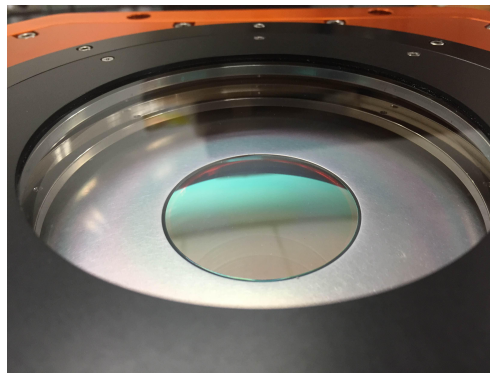


Figure 4. The thermal blocking filter installed in the GLS cryostat inner sanctum lid plate. Currently, an aperture is installed on the inner sanctum (into which the filter is potted), directly over the filter.

3.2 Custom Thermal Blocking Filter

The thermal blocking filter is a *Semrock* interference filter with strong ($\text{OD} > 6$) blocking from 1.3 – 2.1 μm . Multiple independent spectral scans verify the blocking performance of this filter at normal incidence, including *Semrock* verification measurements, measurements by our team using a Perkin-Elmer Lambda 950 UV-Vis spectrophotometer, and point measurements by our team using continuous wave lasers and a photodiode. Figure 3 shows the predicted and measured performance of this filter. Note that measurements of blocking stronger than OD6 (transmission $T < 10^{-6}$) have low signal-to-noise ratios (SNRs), so in regions where measurements vary from OD6-OD10, only a lower limit of $\sim\text{OD}6$ should be understood.

At higher incidence angles, the blocking “spectrum” decreases and shifts blueward somewhat, so that the filter transmits increasingly the red thermal background. However, the good performance is maintained over a large range of incidence angles: even at 30 deg, the filter blocks from 1.3 – 2.0 μm at $\text{OD} > 6$

4. METHOD

By varying the spectrum of light incident on the detector and the properties of the incident beam, we can place constraints on the sensitivity in the Urbach tail spectral region, past the cutoff of $\sim 1.7 \mu\text{m}$. This is possible

due to the strong suppression of the thermal blocking filter, which only transmits at wavelengths shorter than $\sim 1.3 \mu\text{m}$ (where the thermal contribution is relatively small) and longer than the detector cutoff (where the Urbach tail governs the overall efficiency).

We vary the temperature of the heated lid and record the statistics of the thermal signal in an $r \approx 20$ pix circle at the center of the array. A dark frame, recorded with the plate cooled by liquid nitrogen, is subtracted from each dataset.

4.1 Modeling

We modeled the signal at array center using a blackbody source spectrum ($\epsilon = 1$), transmitted through the blocking filter (transmission shown in Figure 3) and detected by the H2RG (QE given by Equations 2). The apertures control the solid angle visible at array center, and the filter degradation at higher incidence angles is accounted for. The signal is integrated within successive one-degree annuli, and circular symmetry is assumed.

To fit the QE function to the (temperature, signal) data, we implemented the *lmfit* Python package[†], which provides a flexible least-squares minimizer. The free parameters of the QE function include the thickness of the HgCdTe layer, the exact cutoff wavelength, and most importantly the Urbach tail parameter w . We used the Nelder-Mead optimization method to find the best fit Urbach tail for each dataset.

5. CURRENT RESULTS AND DISCUSSION

5.1 Basic Expectations

It is instructive to consider the predicted signal in our experiment for two extreme cases of the Urbach tail, with the heated plate at room temperature. For a very sharp Urbach tail ($w = 0.005$ eV, shown in Figure 5), the expected signal at approximately the level of the H2RG dark current ($\sim 0.01 \text{ e s}^{-1} \text{ pix}^{-1}$), which would be very difficult to measure.

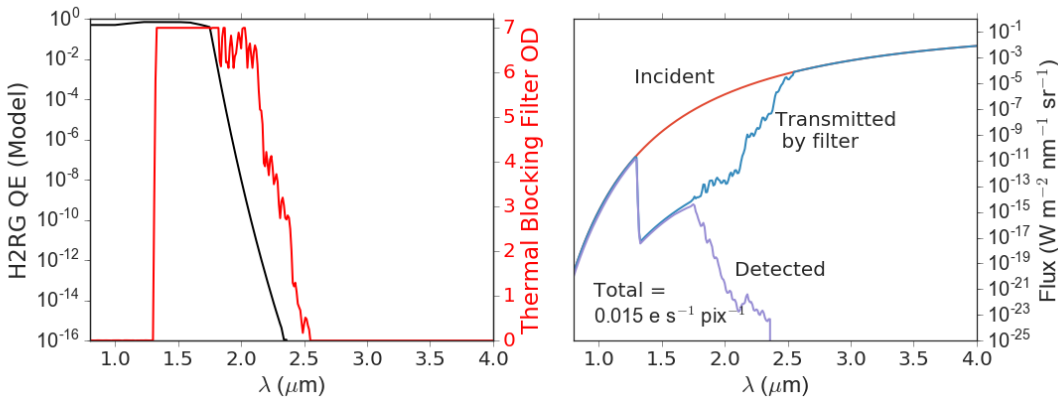


Figure 5. Predicted signal for an H2RG with a sharp cutoff ($w = 0.005$ eV), with the top plate at room temperature.

At the other extreme, an extended Urbach tail ($w = 0.016$ eV, shown in Figure 6) in the same configuration yields orders of magnitude higher signal ($\sim 0.5 \text{ e s}^{-1} \text{ pix}^{-1}$). As discussed below, our multiple measurements at different source temperatures suggests an Urbach tail more consistent with $w = 0.016$ eV than with $w = 0.005$ eV.

5.2 Trial 1: Large Aperture

Trial 1 was carried out with a ~ 24 mm aperture directly above the outer GLS window. If this were the limiting aperture, it would define a beam of approximately F/1.7 (although see discussion in Section 5.5). A least squares fit to the source temperature vs recorded signal data yields an Urbach $w = 0.014$ eV for the F/1.7 beam. The measured data, fit, and corresponding QE curve are shown in Figure 7.

[†]<http://cars9.uchicago.edu/software/python/lmfit/>

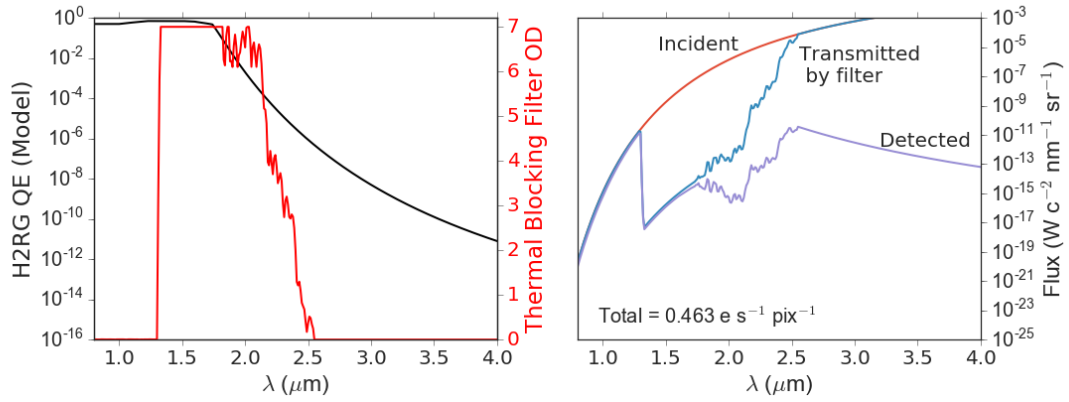


Figure 6. Predicted signal for an H2RG with a shallow cutoff ($w = 0.016 \text{ eV}$), with the top plate at room temperature.

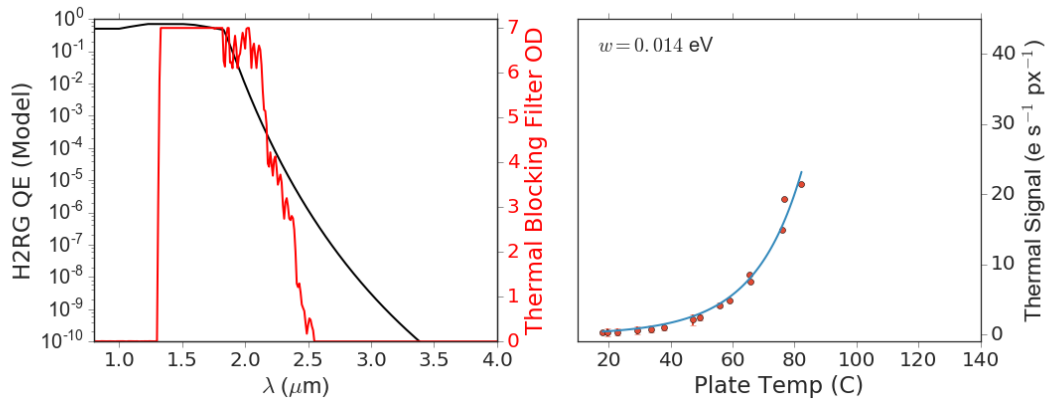


Figure 7. Measured and predicted signal for a range of source temperatures with a $\sim 24 \text{ mm}$ aperture above the GLS window. The best fit Urbach parameter w is shown.

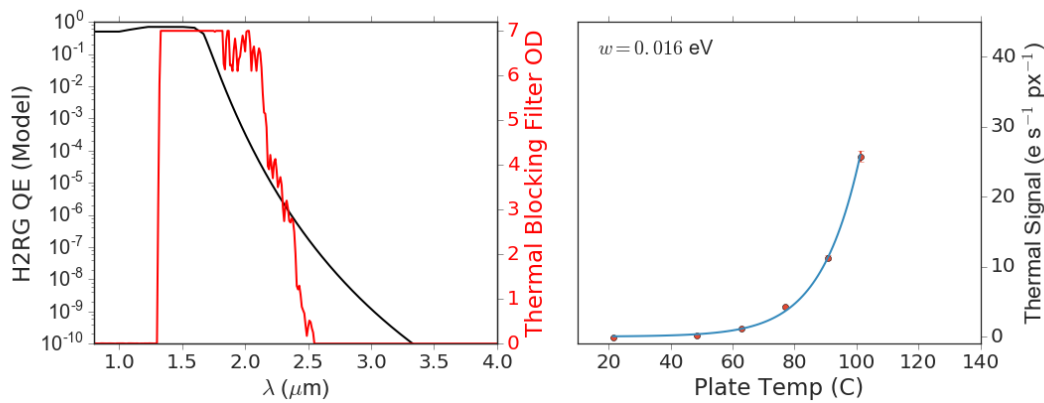


Figure 8. Measured and predicted signal for a range of source temperatures with a ~ 18 mm aperture above the GLS window. The best fit Urbach parameter w is shown.

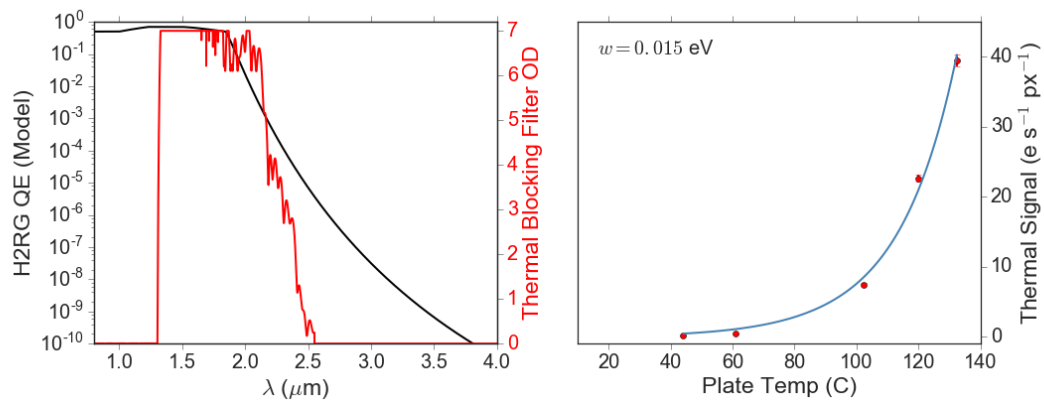


Figure 9. Measured and predicted signal for a range of source temperatures with a ~ 6 mm aperture above the GLS window. The best fit Urbach parameter w is shown.

5.3 Trial 2: Medium Aperture

Trial 2 was carried out with a ~ 18 mm aperture (approximately F/2.1). A least squares fit to the source temperature vs recorded signal data yields an Urbach $w = 0.016$ eV for the F/2.1 beam. The measured data, fit, and corresponding QE curve are shown in Figure 8.

5.4 Trial 3: Small Aperture

Trial 3 was carried out with a ~ 6 mm aperture (approximately F/6). A least squares fit to the source temperature vs recorded signal data yields an Urbach $w = 0.015$ eV for the F/6 beam. The measured data, fit, and corresponding QE curve are shown in Figure 9.

5.5 Experimental Improvements

An important experimental issue remains: the aperture mounted on the inner sanctum is approximately 1 mm in diameter and should limit the beam to a very slow F/14. However, we observe a strong impact on the measured signal when even a relatively large 24 mm aperture is installed and well-aligned above the GLS outer window. Moreover, in the fits discussed above, we are unable to reproduce the measured data with realistic parameters without increasing the range of input angles beyond the F/14 beam expected from the inner sanctum aperture. All fits performed thus far strongly prefer a larger range of incident angles, commensurate with the aperture

above the GLS outer window. We take this to be a likely sign of scattered light or other contamination and are working to improve the control and definition of the input beam.

It is worth noting, however, that these uncertainties about the beam do not affect the qualitative result that the magnitude of thermal signal we measure strongly indicates an extended Urbach tail. Specifically, the basic examples discussed in Section 5.1 are not strongly dependent on the range of incident angle. An extended Urbach tail is needed to explain the observed signal at room temperature and higher.

6. CONCLUSIONS AND FUTURE PROSPECTS

Our measurements with an engineering grade 1.7 μm -cutoff H2RG detector array and a strong thermal blocking filter suggest a red sensitivity tail that extends far beyond the formal cutoff. This has implications for NIR systems being designed and built, as predicted thermal background may be underestimated. It also has implications for the design of potential warm-pupil systems, requiring substantial blocking well past the detector cutoff.

We are working to improve our experimental setup, and to evaluate and control any possible scattered light or other sources of contamination. This work will enable us to more precisely constrain the shape of the Urbach tail, and the severity of its impact in NIR instruments.

ACKNOWLEDGMENTS

This work was partially supported by funding from the Center for Exoplanets and Habitable Worlds. The Center for Exoplanets and Habitable Worlds is supported by the Pennsylvania State University, the Eberly College of Science, and the Pennsylvania Space Grant Consortium. We acknowledge support from NSF grants AST 1006676, AST 1126413, and AST 1310885.

REFERENCES

- [1] R. Blank, S. Anglin, J. W. Beletic, S. Bhargava, R. Bradley, C. A. Cabelli, J. Chen, D. Cooper, R. Demers, M. Eads, M. Farris, W. Lavelle, G. Luppino, E. Moore, E. Piquette, R. Ricardo, M. Xu, and M. Zandian, “H2RG focal plane array and camera performance update,” *Proc. SPIE* **8453**, p. 845310, 2012.
- [2] A. Rogalski, “HgCdTe infrared detector material: history, status and outlook,” *Reports on Progress in Physics* **68**(10), pp. 2267–2336, 2005.
- [3] Y. Chang, G. Badano, J. Zhao, Y. D. Zhou, R. Ashokan, C. H. Grein, and V. Nathan, “Near-bandgap infrared absorption properties of HgCdTe,” *Journal of Electronic Materials* **33**(6), pp. 709–713, 2004.
- [4] F. Urbach, “The long-wavelength edge of photographic sensitivity and of the electronic Absorption of Solids,” *Physical Review* **92**(5), p. 1324, 1953.
- [5] E. Finkman and S. E. Schacham, “Exponential optical absorption band tail of HgCdTe,” *Journal of Applied Physics* **56**(10), pp. 2896–2900, 1984.
- [6] J. Chu, B. Li, K. Liu, and D. Tang, “Empirical rule of intrinsic absorption spectroscopy in $\text{Hg}_{1-x}\text{Cd}_x\text{Te}$,” *Journal of Applied Physics* **75**(2), pp. 1234–1235, 1994.
- [7] Y. Chang, S. Guha, C. H. Grein, S. Velicu, M. E. Flatt e, V. Nathan, and S. Sivananthan, “Absorption of narrow-gap HgCdTe near the band edge including nonparabolicity and the Urbach tail,” *Journal of Electronic Materials* **36**(8), pp. 1000–1006, 2007.
- [8] J. Chen, M. Loose, R. Ricardo, J. Beletic, M. Farris, M. Xu, A. Wong, and C. Cabelli, “SIDE CAR ASIC firmware for astronomy applications,” *Proc. SPIE* **9154**.
- [9] P. R. McCullough, M. Regan, L. Bergeron, and K. Lindsay, “Quantum Efficiency and Quantum Yield of an HgCdTe Infrared Sensor Array,” *Publications of the Astronomical Society of the Pacific* **120**(869), pp. 759–776, 2008.